Supplemental Appendix for "Three-Dimensional Single-Molecule Fluorescence Imaging Beyond the Diffraction Limit Using a Double-Helix Point Spread Function"

Sri Rama Prasanna Pavani[1†], Michael A. Thompson[2†], Julie S. Biteen[2], Samuel J. Lord[2], Na Liu[3], Robert J. Twieg[3], Rafael Piestun[1*], and W. E. Moerner[2*]

[1]Department of Electrical and Computer Engineering, University of Colorado, Boulder, CO 80309
[2]Department of Chemistry, Stanford University, Stanford, California 94305
[3]Department of Chemistry, Kent State University, Kent, OH 44242
† Equal contributions
*To whom correspondence should be addressed

CONTENTS

A. Point spread function engineering

The double-helix point spread function (DH-PSF) exhibits two prominent lobes that rotate with axial propagation. This PSF is related to a class of propagation-invariant rotating beams, which are obtained by superposing optical modes that fall along a line in the Gauss-Laguerre (GL) modal plane(1). Because an exact line-superposition results in an extremely absorptive mask, an iterative optimization procedure operating in three different domains (GL modal plane, Fourier, and spatial) is used to design the photon-efficient DH-PSF phase-mask (SA Fig. 1a) that was used in the experiments reported in this paper.

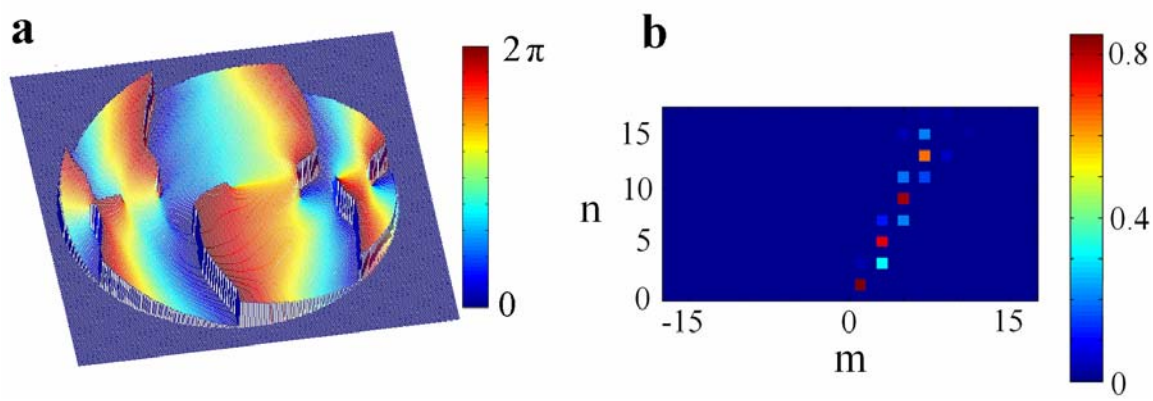

SA Fig. 1: DH-PSF design produced from iterative optimization. (a) DH-PSF phase mask exhibiting 7 phase singularities, (b) the GL modes constituting the mask form a cloud in the GL modal plane. (m, n) are the indices of the GL modes(1).

Briefly, the PSF design optimization enforced that a phase-only transfer function generated an on-axis DH-PSF, whose lobes exhibit not more than a 180° rotation along the focal region, while carrying maximum PSF energy in them(2). With an understanding of the significance of the phase of GL modes over their amplitude, the design procedure expanded the degrees of freedom in the GL modal plane (SA Fig. 1b) to simultaneously satisfy all of the above constraints. This resulted in a DH-PSF phase mask with over 30 times higher transfer-function efficiency compared to the perfectly propagation-invariant superposition, thereby enabling the use of the DH-PSF in photon-limited applications.

The in-focus DH-PSF lobes are about 1.7 times larger and are separated by about 3 times the size of a corresponding in-focus standard PSF lobe. While the DH-PSF expands by roughly 1.2 times through its range of operation, the standard PSF expands by about 9.6 times through this range.

B. Gaussian Estimation Scheme in Figure 2

In order to best assess the localization precision with the DH-PSF system, we developed a more complex nonlinear fitting algorithm for the molecule in Figure 2 than the one used for Figures 3 and 4. Each lobe was identified and isolated with a $(9 \text{ pixel})^2$ box. The lobes in the PSF were then each fit to a 2-D Gaussian using the MATLAB function, nlinfit, to extract an estimate of the center position of each lobe. Then the

standard procedure for finding the x, y, and z positions of the molecule was applied, that is, using the angle of the line between the two lobe positions to extract z, and the midpoint to extract x and y. If the lobes of the PSF are symmetric, then this fitting procedure can give better results than a simple centroid fit, although it is significantly more complex computationally. For this molecule it offers a 15% improvement in localization precision in all three directions over the simpler centroid fit algorithm. For the large number of single molecules in Figures 3 and 4, we chose to use a centroid fitting scheme (described in the next section) both because the improvement is not overly significant for most molecules and because the centroid takes up less computational time.

In addition, for the data in Figure 2, a 100 nm fluorescent bead (Fluospheres 565/580, Molecular Probes, Inc.) was used as a fiduciary marker. Because the bead emits many more photons, its localization precision is much better than for a single molecule. SA Figure 2 shows the position fluctuations of the bead (b) and the molecule (a), and the dramatic improvement in z estimation drift (c) that results from subtracting the bead motion from the single-molecule z-estimations.

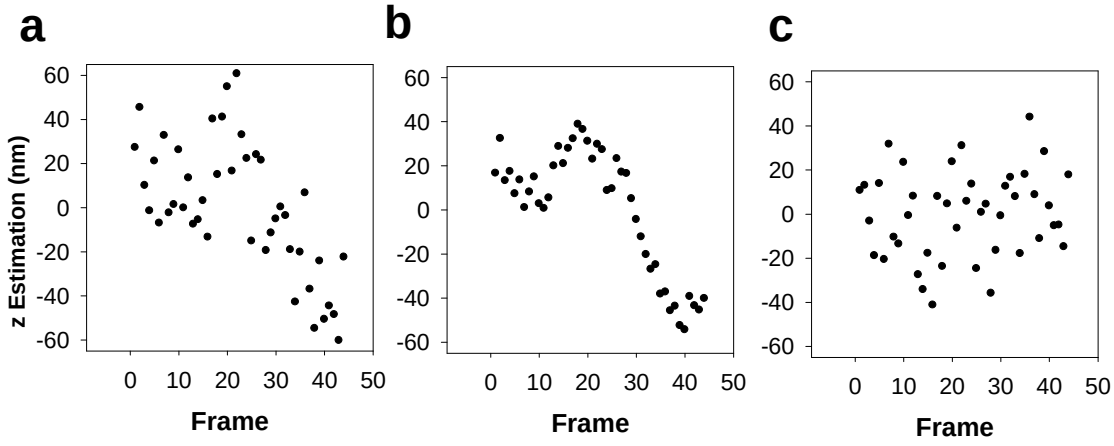

SA Fig. 2 : (a) Estimations of the z position of the DCDHF-V-PF_4 molecule featured in Fig. 2 of the main text. (b) Estimations of the z position of the fluorescent bead fiduciary in the sample, illustrating the z drift of the microscope and/or the z-piezo. (c) Fiduciary-corrected positions of the single molecule.

C. Estimation Algorithm for 3-D Images (Figs. 3, 4)

Each frame of the raw detected movies shows multiple molecules located over a transverse-position-dependent background that resembles the Gaussian intensity profile of the excitation beam. 3D positions of the molecules in each of these frames are estimated with an algorithm implemented in MATLAB. The algorithm first finds the coarse molecule positions from the raw image, and then zooms in on these coarse positions to find the exact 3D positions as explained below.

The non-uniform background prohibits the use of direct thresholding to identify molecules in the raw detected image. Hence, we used an edge detection algorithm that calculates the modulo-square of the gradient of the raw image to locate the coarse molecule positions. The gradient distinguishes the molecules from the slowly varying background by highlighting the edges around the molecules' response. The centroid of the area enclosed by the edges of a molecule is taken as the molecule's coarse x and y position. A $(19 \text{ pixel})^2$ region centered about the coarse position is then extracted out to find the exact 3D molecule position. The two DH-PSF lobes present within this region are separated from the background using an adaptive thresholding technique. This technique finds the smallest threshold above the background such that the areas of the two lobes are maximized while remaining disconnected. The photon counts used for the colormap of Fig. 3 and in the horizontal axis of SA Fig. 3 are the photons counted from these maximum lobe-areas after background correction. The centroid coordinates of the two DH-PSF lobes were then computed. The axial position of the molecule was estimated by mapping the angle between the two centroid locations to axial distance using the calibration plot shown in Fig. 1 of the main text. The transverse molecule positions were estimated from the midpoint of the centroids of the DH-PSF lobes after applying a z-dependent transverse correction. This correction compensates for a small systematic change in tranverse position of the DH-PSF lobe centroid midpoint as a function of z, determined from fluorescent bead imaging with z-focus displacement produced by the piezo.

This estimation algorithm finally generated a 4D (3D spatial - temporal) dataset containing the molecule positions from different camera frames. This matrix was directly displayed in Fig. 3 of the main text. In Fig. 4, the temporal dimension was squeezed by

replacing multiple localizations of a molecule within an activation cycle with the mean estimate. The precisions shown in the vertical axis of SA Fig. 3 are the standard deviations of estimates of the position for multiple molecules obtained from the above 4D dataset after a drift correction based on correlation analysis of the single-molecule positions, which compensated for any linear stage drift along any of the three dimensions.

D. Localization precision as a function of the number of detected photons

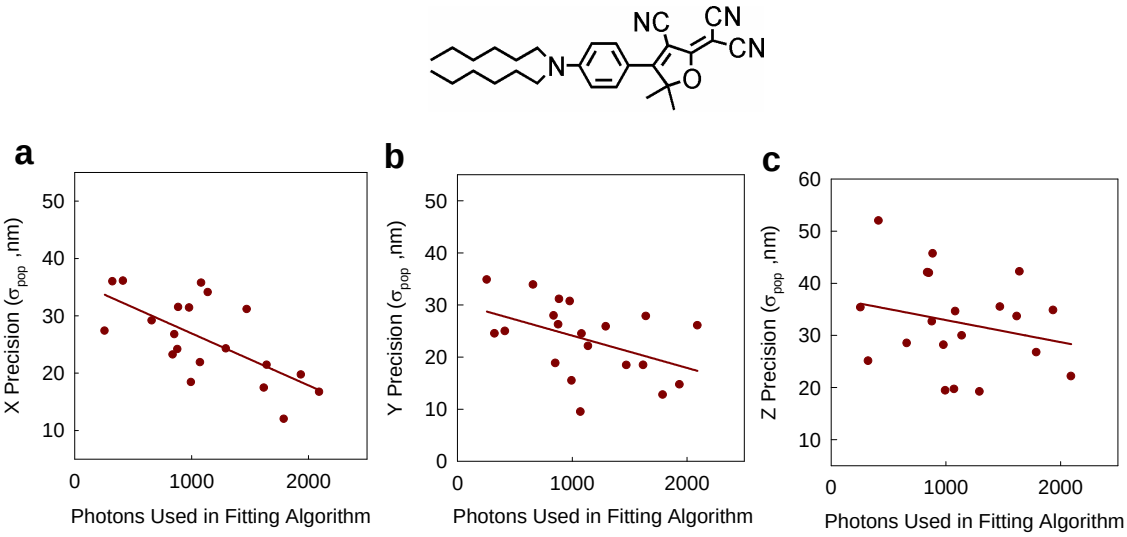

SA Fig. 3: The localization precision from single DCDHF-P (structure shown) molecules as a function of the number of photons used in the centroid estimation algorithm for the x (a), y (b), and z (c) directions. All measurements were made with acquisition times of 500 ms and the rms background noise in the samples was approximately 20 photons/pixel.

SA Fig. 3 shows three plots of the localization precision for multiple localizations of different DCDHF-P(3) molecules versus the number of photons used in the fitting algorithm for that molecule. The ordinate of each plot refers to the localization precision as defined by the standard deviation of the population of molecule location measurements as illustrated in Fig. 2a, which can be regarded as the localization precision expected for a single position determination. The data in SA Fig. 3 was obtained using the computationally simpler centroid fitting scheme described in the previous section. The centroid estimation algorithm does not use all of the photons in the DH-PSF, but rather applies an adaptive threshold that only uses photons in the primary two lobes above a

certain background level. This is in contrast to the fitting algorithm used in Figure 2, which does not threshold the data and hence uses all available photons to find the position of the molecule. There is a weak and seemingly linear negative correlation between the localization precision and number of photons, but a full analysis of this and the development of an optimal estimation algorithm are subjects of future work. A possible reason for the scatter is that the DH-PSF shape can change slightly depending on the axial position of the emitter, that is, one lobe appears better defined than the other at certain axial positions, possibly arising from aberration effects. Another reason is that the background fluctuations from position to position are partly deterministic: because much of the background itself is actually weak, the sidelobes from the various GL modes forming the PSF combine to make a widely spatially varying, but temporally constant, variation across the sample.

E. Calibration of CCD gain for photon counting

In order to convert EMCCD camera counts to photons, two calibrations are required: the conversion gain, (number of e^- after on-chip gain)/(ADC count), and the electron multiplication gain (number of e^- after on-chip gain)/(number of photoelectrons). The conversion gain was calibrated according to a previously published procedure(4). Briefly, the method proceeds as follows. First, one records two images of a dim uniform field (a blank, clean coverslip) at the same light intensity level with no EM gain for an arbitrary number of evenly spaced intensities. Due to Poisson fluctuations in detected photons, a plot of the variance of the image for each intensity level versus the mean signal of the image for each intensity level should be a straight line with a slope that equals the inverse of the conversion gain. Significant flat-field effects due to nonuniformity in pixel sensitivity caused a nonlinear dependence and they were removed by two methods described in reference 4.

The electron multiplication gain on the camera needs to be calibrated because the value selected in the software does not always exactly match the true value. To calculate this factor for any software input value, we measured the ratio of the mean signal under an arbitrary irradiance and the mean signal with the camera shutter closed. Because dark

counts are negligible, the electron multiplication gain is then determined by computing this ratio with the gain on divided by this ratio with the gain off (i.e., multiplicative gain=1).

F. Synthesis of photoactivatable fluorophore DCDHF-V-PF_4-azide

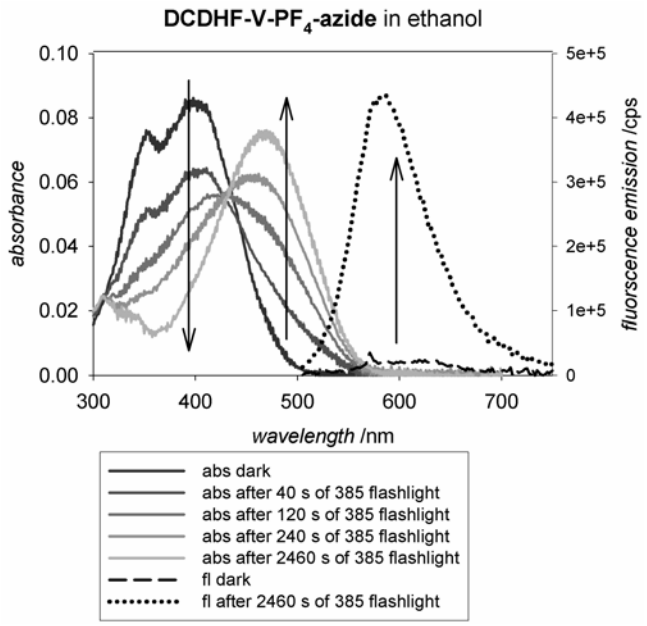

SA Fig. 4: Absorption (solid lines) and fluorescence (dashed and dotted lines) spectra of the DCDHF-V-PF_4-azide dark fluorogen before and after photoactivation to the amino fluorophore. The short-wavelength absorption peak, which corresponds to the azido fluorogen, disappears after illumination with 385-nm light (0.3 mW/cm^2); the longer wavelength peak of the fluorescent amino compound grows in. Before photoactivation, pumping at 490 nm yields little fluorescence (dashed line); after activation with 385-nm illumination, pumping at 490 nm produces much brighter fluorescence (dotted line).

4-Azido-2,3,5,6-tetrafluorobenzaldehyde(5-8)

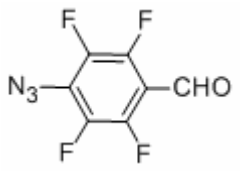

To a 100-mL round-bottom flask with stirbar was added pentafluorobenzaldehyde (1.96 g, 0.01 mol), sodium azide (0.72 g, 0.011 mol), acetone (15 mL) and water (15

mL). The mixture was warmed to reflux under nitrogen for 10 h. TLC showed all the pentafluorobenzaldehyde was consumed and so the reaction was stopped and cooled to room temperature. The product mixture was diluted with 20 mL of water. The crude product was extracted with ether (30 mL ×5). The combined organic layer was dried over anhydrous $MgSO_4$. The solvent was removed at room temperature under vacuum. Sublimation of the residue (50 ºC/0.2 mm) gave the final product as a white solid (1.20 g, 55% yield). Mp 44 ºC (lit 44–45 ºC, ref (5)). IR (neat): 3377, 2121, 1704, 1644, 1480, 1398, 1237, 1066, 1000, 615 cm^{-1}. ^1H NMR (400 MHz, $CDCl_3$): δ 10.26 (m, 1H); ^{19}F NMR (470 MHz, $CDCl_3$): δ –149.6 (m, 2F), –155.6 (m, 2F).

(*E*)-2-(4-(4-Azido-2,3,5,6-tetrafluorostyryl)-3-cyano-5,5-dimethylfuran-2(5*H*)-ylidene)malononitrile (DCDHF-V-PF_4-azide)

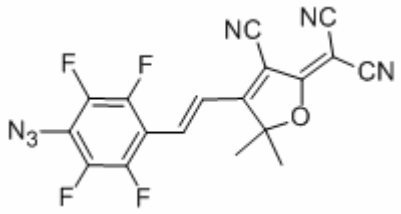

To a 100-mL round-bottom flask with stirbar was added 4-azido-2,3,5,6-tetrafluoro-benzaldehyde (0.22 g, 1 mmol) and 2-(3-cyano-4,5,5-trimethyl-5*H*-furan-2-ylidene)-malononitrile (0.22 g, 1.1 mmol), 5 mL pyridine and several drops of acetic acid. The mixture was stirred at room temperature for 2.5 days. TLC showed the desired azido product had been formed as the main product. The reaction was stopped and poured into 500 mL ice-water. After stirring for 2 h, the precipitate was filtered off by suction filtration. The solid was recrystallized from 1-propanol. After recrystallization, part of the azido product was converted to the corresponding amino compound. The mixture was adsorbed on silica gel, placed at the top of a silica column and eluted (CH_2Cl_2:EtOAc = 20:1). Fractions containing only the first product were combined and concentrated to give an orange product (40 mg, 10% yield). This is the final azido product, (*E*)-2-(4-(4-azido-2,3,5,6-tetrafluorostyryl)-3-cyano-5,5-dimethylfuran-2(5*H*)-ylidene)malononitrile.
Recrystallization could not be done on this compound, since it has high photoreactivity: it readily converts to the corresponding amino compound in solvents (like propanol) in daylight. IR (neat): 2933, 2228, 2124, 1586, 1557, 1489, 1372, 1253, 998 cm^{-1}. ^1H NMR

(400 MHz, $CDCl_3$): δ 7.63 (d, *J* = 16.8 Hz, 1H), 7.31 (d, *J* = 16.4 Hz, 1H), 1.82 (s, 6H); ^{13}C NMR (100 MHz, $CDCl_3$): δ 174.5, 172.5, 146.9 (m), 144.4 (m), 142.0 (m), 139.4 (m), 130.7, 121.4 (t, *J* = 9.8 Hz), 111.1, 110.3, 109.5, 102.6, 97.8, 51.3, 26.3; ^{19}F NMR (470 MHz, $CDCl_3$): δ –143.5 (2F), –155.2 (2F). UV–vis (EtOH): λ_{max} = 406 nm, ε = 2.7 x 10^4 L mol^{-1} cm^{-1}.

References

1. Piestun R, Schechner YY & Shamir J (2000) Propagation-invariant wave fields with finite energy. *J. Opt. Soc. Am. A* 17, 294-303.

2. Pavani SRP & Piestun R (2008) High-efficiency rotating point spread functions. *Opt. Express* 16, 3484-3489.

3. Willets KA, Ostroverkhova O, He M, Twieg RJ & Moerner WE (2003) New fluorophores for single-molecule spectroscopy. *J Am Chem Soc* 125, 1174-1175.

4. Newberry M (1998) Mirametrics technical note on pixel response effects in CCD camera gain calibration http://www.mirametrics.com/tech_note_ccdgain.htm

5. Keana JFW & Cai SX (1990) New reagents for photoaffinity labeling: Synthesis and photolysis of functionalized perfluorophenyl azides. *J Org Chem* 55, 3640-3647.

6. Keana JFW & Xiong Cai S (1989) Functionalized perfluorophenyl azides: New reagents for photoaffinity labeling. *Journal of Fluorine Chemistry* 43, 151-154.

7. Stromgaard K, *et al* (2002) Ginkgolide derivatives for photolabeling studies: Preparation and pharmacological evaluation. *J Med Chem* 45, 4038-4046.

8. Michaela Wiegand TKL, (2006) Synthesis of photoactive alpha-mannosides and mannosyl peptides and their evaluation for lectin labeling. *European Journal of Organic Chemistry* 2006, 4841-4851.